RSC Advances

ROYAL SOCIETY OF CHEMISTRY

www.rsc.org/advances

Synthesis and characterization of lysine-modified SBA-15 and its selective adsorption of scandium from a solution of rare earth elements

Jiaxian Ma[a,b], Zheng Wang[*,b], Ying Shi[a], Qing Li[b]

A novel lysine-functionalized mesoporous material (Fmoc-SBA-15) was synthesized using a facile two-step post-grafting method to obtain an adsorbent that can selectively adsorb scandium from aqueous solution. The ordered mesoporous structure of the material was confirmed by powder X-ray diffraction (XRD), transmission electron microscopy (TEM) analysis, and N_2 adsorption–desorption isotherms. The Fourier transform infrared (FT-IR) spectroscopy confirmed that lysine was introduced into SBA-15. Furthermore, the materials showed an excellent scandium adsorption capacity (35.29 mg g^{-1}) at room temperature with a scandium uptake time of <10 min. The adsorption isotherms and uptake kinetics were also investigated. The equilibrium data were better represented by the Freundlich isotherm model than by the Langmuir model. The pseudo-second-order kinetics model best described the adsorption kinetics of scandium ions onto Fmoc-SBA-15. Moreover, the material possessed high selectivity for scandium from a rare earth element solution.

INTRODUCTION

Scandium (Sc) is widely used in the chemical, glassware, spaceflight, nuclear technology, laser, computer power, superconductor, and medical treatment industries[1,2]. However, it is rare and expensive because of its scarce resources and difficulties associated with its extraction. In particular, as a typical scattered lithophile element, Sc scarcely exists as an independent mineral[4]. It is primarily found in rare earth mines in China. Furthermore, the separation of Sc from other rare earth elements (REEs) is difficult, because REEs all have very similar chemical properties. Therefore, complicated flow sheets are needed to obtain high-purity Sc products, which greatly increases the operating costs[3]. Consequently, the commercial applications of Sc are limited.

On the other hand, with the large-scale and rapid increases in the exploitation of REE resources and the wide application of REE-enriched fertilizers as growth promoters in agriculture, the contamination levels of soil and water around mining areas have increased substantially[5-7]. Furthermore, excessive REE concentrations in the soil may have a serious impact on the surrounding ecosystems, groundwater, agricultural productivity, and, ultimately, human health through the presence of REEs in the food chain[8,9]. Previous studies have found that REEs are accumulated in the blood, brain, and bone after entering into the human body[10-12], which may result in health problems such as declines in liver function[13,14]. Therefore, it is necessary to determine the concentration of trace REEs in natural water sources. For this purpose, in recent years, much effort has been devoted to seeking out new materials with high adsorption capacities for Sc in particular, as a representative REE[15-17]. Because the concentration of Sc in natural water sources can be very low[18], it is normally necessary to preconcentrate the solution before determination. Thus, it is meaningful to prepare a material which can be used in not only the preconcentration of Sc, but also the separation of Sc from the REE pollution.

The main methods for Sc separation are liquid–liquid extraction[19,20], ion-exchange chromatography[21], and extraction chromatography[22]. Although these methods are highly practical for the separation of Sc, their procedures are complicated by multistage cycles, extractant loss, the formation of stable emulsions, long separation times, and other problems. Moreover, poisonous reagents such as toluene are introduced in extraction processes and might cause secondary pollution. Conversely, adsorption is a promising method for recovering trace metals in polluted water, and adsorbents play an important role in determining the adsorption efficiency. For example, under suitable experimental conditions, chemically stable metal chelates can be formed between ions and reagents comprising β-diketone and amino groups[23,24]. In particular, based on the hard-soft acid base theory, a successful attempt was made to synthesize acetylacetone-modified silica gel and ethylenediaminetriacetic acid-functionalized copolymeric resin in order to adsorb REEs[15, 25]. These materials were capable of adsorbing various REEs, but unfortunately, they could not selectively adsorb Sc.

It is known that the mesoporous silica SBA-15 can selectively adsorb metals if particular groups are grafted on the SBA-15 surface[26-30]. In addition, mesoporous SBA-15 can provide a stable mesoporous support structure with hexagonally packed cylindrical channels, thick pore walls, and good dispersibility in aqueous solutions. Moreover, the profusion of silanol groups on the surface allows for both organic modification and applications in metal adsorption[31-35]. In particular, *N*-α-Fmoc-*N*-ε-Boc-*L*-lysine is an accessible and nontoxic biomolecule with many electron-attracting groups such as carbonyl groups and multiple amino groups. In fact, carboxyl groups on this lysine easily react with amino groups on NH_2-SBA-15. Previously, the aforementioned REE adsorbents have been synthesized with derivatives of β-diketone such as acetylacetone[15], which are always toxic and are not very cost effective. Therefore, lysine-functionalized mesoporous silica can provide a meaningful nontoxic treatment method for the preconcentration of Sc.

To the best of our knowledge, there have been no related studies on mesoporous materials adsorbing Sc reported so far. In the present study, we obtained highly ordered hexagonal SBA-15 bearing lysine using a post-grafting method. Powder X-ray diffraction (XRD), transmission electron microscopy (TEM) analysis, N_2 adsorption–desorption isotherms, and Fourier

transformed infrared (FT-IR) spectroscopy were used to characterize the material. We first studied the adsorption behaviour of REEs using SBA-15, NH_2-SBA-15, and Fmoc-SBA-15, with a particular focus on the selective adsorption of Sc from a mixed REE solution. Then, the Sc adsorption on the lysine-modified adsorbent was investigated in terms of the Sc static adsorption capacity and uptake kinetics.

EXPERIMENTAL SECTION

Reagents and materials

Poly(ethylene glycol)-block-poly(propylene glycol)-block-poly(ethylene glycol) (P123, M_{av} = 5800) and (3-aminopropyl)-triethoxysilane (APTES) were obtained from Sigma-Aldrich, America. Tetraethoxysilane (TEOS), *N*-α-Fmoc-*N*-ε-Boc-*L*-lysine (99%, M_{av} = 468), HNO_3, HCl, and $NH_3 \cdot H_2O$ solutions were obtained from Shanghai Sinopharm Chemical Reagent Co., Ltd., China. Dicyclohexylcarbodiimide (DCC) and 4-dimethylaminopyridine (DMAP) were obtained from Shanghai Medpep Co., Ltd., China.

Organic solvents such as toluene, ethanol, pyridine, trifluoroacetic acid (TFA), dichloromethane (DCM), and dimethylformamide (DMF) were obtained from Shanghai Sinopharm Chemical Reagent Co., Ltd., China. Before use, the toluene, ethanol, and dimethylformamide (DMF) were dried overnight with activated 4A-type molecular sieves.

The REE solutions were obtained by diluting the stock standard solutions (0.1 g L^{-1}) (Inorganic Ventures Co., Ltd., America) with deionized water. The Sc ion solution was obtained by dissolving scandium oxide (Johnson Matthey Co., Ltd., England) with HCl and deionized water. The deionized water (resistance 18.25 MΩ·cm) used was obtained from Millipore, Bedford, MA, America. The glassware was soaked in (1+1) HCl overnight and cleaned with Milli-Q water before use. All reagents were at least analytical grade.

Synthesis of functionalized mesoporous silica

SBA-15 and NH_2-SBA-15 were prepared following the method used in our previous study[36,37]. The grafted lysine-modified mesoporous silica was synthesized by reacting NH_2-SBA-15 and *N*-α-Fmoc-*N*-ε-Boc-*L*-lysine. Note that we used *N*-α-Fmoc-*N*-ε-Boc-*L*-lysine as a reactant primarily because the side reaction between lysine molecules had a serious impact on the rate of the main reaction, and there is no similar side reaction between *N*-α-Fmoc-*N*-ε-Boc-*L*-lysine molecules. For subsequent experiments, the Boc group has to be removed because its strong hydrophobicity may seriously affect the adsorption properties of the material for the target ion. However, it is unnecessary to remove the Fmoc group because it contains carbonyl groups, which are electron-attracting. To optimize the Sc adsorption capacity, we synthesized four lysine-modified mesoporous silica samples. Approximately 1 g of NH_2-SBA-15 was added to 200 mL of the solvent DMF with 3.08 g of DCC, 0.05 g of DMAP, and 4 g, 5 g, 6 g, or 7 g of *N*-α-Fmoc-*N*-ε-Boc-*L*-lysine. The mixture was refluxed at 80°C for 24 h in a nitrogen atmosphere. Based on the Sc adsorption capacity, the optimal *N*-α-Fmoc-*N*-ε-Boc-*L*-lysine dosage was determined to 6 g. The resulting solids were filtered out, washed with DMF and ethanol successively, and dried in an air atmosphere at 60°C for 10 h. The sample was named lysine-SBA-15.

Finally, to remove the hydrophobic *t*-butyloxycarbonyl (Boc) group, 0.5 g of lysine-SBA-15 was dissolved in 16 mL of DCM and 4 mL of TFA by stirring for 2 h at room temperature. The resulting solids were filtered out, washed successively with deionized water and ethanol, and dried in an air atmosphere at 60°C for 5 h. The sample was named Fmoc-SBA-15. Scheme 1 shows the synthesis routes for this material.

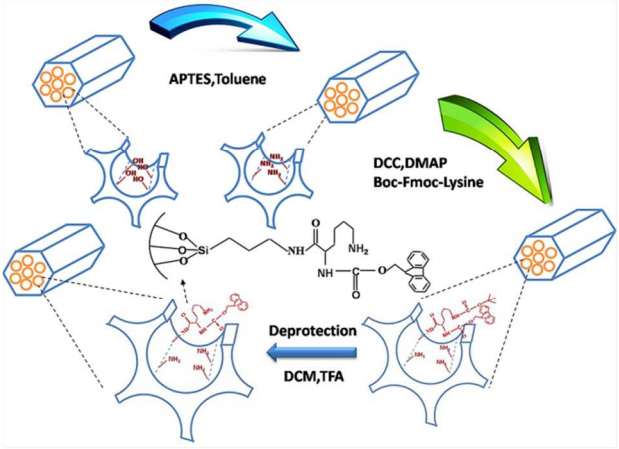

Scheme 1 Synthesis routes for Fmoc-SBA-15.

Characterization

Powder XRD patterns were collected on a Rigaku D/Max 2200PC diffractometer (Japan Rigaku Corporation, Japan) using Cu K_α radiation at 40 kV and 40 mA. The TEM images were recorded on a JEOL 200CX Electron Microscope (JEOL, Japan) at 160 kV. The N_2 adsorption-desorption isotherms were measured at 77 K on a Micromeritics TriStar 3000 V6.05A analyser (Micromeritics, America). The sample was degassed at 300°C for 5 h before the measurements. Specific surface areas were calculated using the Brunauer-Emmett-Teller (BET) method under a relative pressure ranging from P/P_0 = 0.05 to 0.3. The pore size distribution was obtained using the Barrett-Joyner-Halenda (BJH) method. The pore volumes were obtained from the volumes of N_2 adsorbed at or near P/P_0 = 0.99. The IR spectra were collected using an FTIR Nicolet 6700 spectrometer.

The chemical composition of the water solutions was analyzed using inductively coupled plasma-atomic emission spectroscopy (ICP-AES) (Varian Vista AX, America). The pH was measured using a PHS-3E digital pH meter (Shanghai Precision and Scientific Instrument, China).

Adsorption experiments

The multi-element adsorption experiments were performed as follows: 5 mg of adsorbent was added into 20 mL of an aqueous solution containing REEs (0.1 mg L^{-1}) and stirred at room temperature. The single-element adsorption experiments were performed as follows: 5 mg of adsorbent was added into 20

mL of an aqueous solution containing Sc (1–60 mg L^{-1}) and stirred at room temperature. For both single- and multi-element adsorption experiments, the pH of the solution was adjusted using aqueous HNO_3 and $NH_3 \cdot H_2O$. The mixture was then filtered, and the concentrations of residual REE ions in the solution were determined by ICP-AES.

The adsorbed mass of the REEs was calculated based on the difference between the initial and final solution concentrations. The adsorption capacity q (in mg g^{-1}) of the metal ions adsorbed was calculated using the following equation:

$$q = \frac{(C_0 - C_e)V}{M} \qquad (1)$$

where C_0 and C_e are the initial and equilibrium concentrations of the metal ions in the testing solution (mg L^{-1}), V is the volume of the testing solution (L), and M is the mass of the adsorbent (g).

We used four models to illustrate the adsorption mechanism: the pseudo-first-order kinetic model, pseudo-second-order kinetic model, Langmuir isotherm model, and Freundlich isotherm model. The related equations are described below.

The pseudo-first-order kinetic model can be written as follows:

$$\frac{d_{q_t}}{d_t} = k_1(q_e - q_t) \qquad (2)$$

Here, the linear expression can be represented as

$$\lg(q_e - q_t) = \lg q_e - \frac{k_1}{2.303} t \qquad (3)$$

where q_e and q_t are the adsorption capacity at equilibrium and at time t, respectively (mg g^{-1}), and k_1 is the rate coefficient of pseudo first-order adsorption (L min^{-1}). The q_e and k_1 values were calculated from the plot of $\lg(q_e - q_t)$ with respect to time.

The pseudo-second-order adsorption kinetic rate equation is expressed as

$$\frac{dq_t}{d_t} = k_2(q_e - q_t)^2 \qquad (4)$$

This rate equation can also be represented with a linear expression:

$$\frac{t}{q_t} = \frac{1}{k_2 q_e^2} + \frac{t}{q_e} \qquad (5)$$

Here, k_2 (g (mg min)$^{-1}$) is the rate constant of the pseudo-second-order adsorption. The derivation of the pseudo-second-order kinetic model is based on the notion that the adsorption is related to the squared product of the difference between the equilibrium number of adsorptive sites available on an adsorbent and the number of occupied sites.

The Langmuir isotherm equation can be represented as follows:

$$q_e = \frac{q_m b C_e}{1 + b c_e} \qquad (6)$$

where b is the Langmuir adsorption constant. The linear form of this expression is

$$\frac{c_e}{q_e} = \frac{1}{b q_m} + \frac{c_e}{q_m} \qquad (7)$$

Finally, the Freundlich isotherm equation can be represented by

$$q_e = K_F C_e^{1/n} \qquad (8)$$

The linear form can be written as

$$\lg q_e = \lg K_F + \left(\frac{1}{n}\right) \lg C_e \qquad (9)$$

where C_e (mg L^{-1}) is the equilibrium concentration of the solute, q_e (mg g^{-1}) is the equilibrium adsorption capacity of the adsorbent, and q_m (mg g^{-1}) is the maximum adsorption capacity. The Freundlich adsorption constants are K_F (L g^{-1}) and n.

RESULTS AND DISCUSSION

Characterization of Fmoc-SBA-15

XRD and TEM

The small-angle XRD patterns of SBA-15, NH_2-SBA-15, and Fmoc-SBA-15 are illustrated in Fig. 1. The SBA-15 and NH_2-SBA-15 patterns contain one intense peak at (100) and two small, well-resolved peaks at (110) and (200), describing the well-ordered two-dimensional (2D) structure with hexagonal symmetry that is typical for the highly ordered SBA-15 mesoporous structure. The Fmoc-SBA-15 pattern showed only the intense peak at (100), which indicates that the ordering of the mesoporous structure decreased with increasing concentrations of functional groups. The intensities of the XRD peaks for NH_2-SBA-15 and Fmoc-SBA-15 were slightly lower than those measured for SBA-15. This is evidence that the functionalization primarily occurred inside the mesopore channels, probably caused by the pore filling effect of the SBA-15 channels or by the anchoring ligands on the surface of SBA-15[38, 39].

The TEM images of the Fmoc-SBA-15 sample obtained with the electron beams parallel and perpendicular to the pore channels are shown in Fig. 2. These findings were consistent with the XRD results, indicating that the modified materials maintained their well-ordered mesoporous structure after grafting.

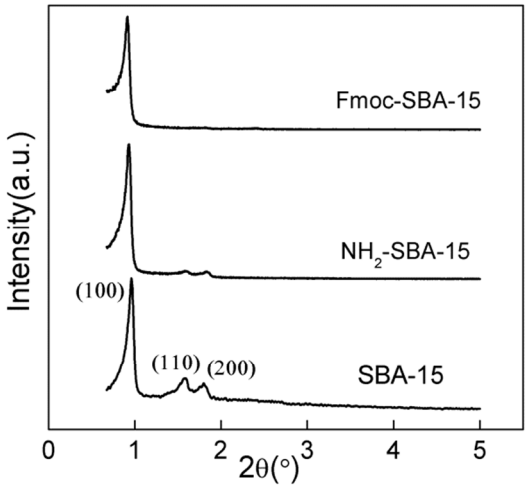

Fig. 1 Small-angle XRD patterns of unmodified SBA-15, NH_2-SBA-15, and Fmoc-SBA-15.

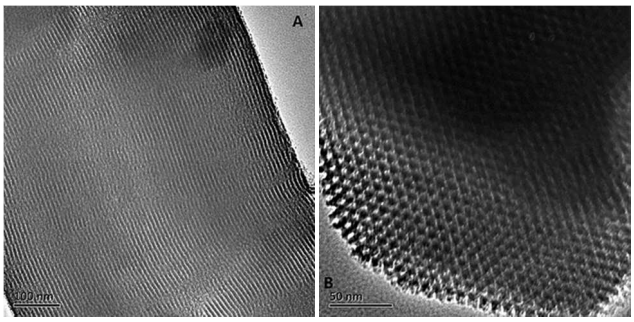

Fig. 2 TEM images of the Fmoc-SBA-15 sample obtained with electron beams (A) parallel and (B) perpendicular to the pore channels.

N_2 adsorption–desorption isotherms

The N_2 adsorption-desorption isotherms of SBA-15, NH_2-SBA-15, and Fmoc-SBA-15 are of Type IV, as shown in Fig. 3. The adsorption and desorption branches of the isotherms for these three materials all exhibited parallel and vertical loops classified as H1 loops, which are a characteristic of materials with a cylindrical pore geometry and a high degree of pore size uniformity. Thus, the uniform mesoporous nature of the material was preserved even though grafting had occurred. The calculated specific surface area (S_{BET}) of these materials decreased from 675 $m^2\ g^{-1}$ to 223 $m^2\ g^{-1}$, and the pore diameter (D_{BJH}) calculated using the BJH method also decreased. These decreases are probably due to the increase in the amount of organic groups inside the SBA-15 channels[39]. The corresponding structural parameters are summarized in Table 1.

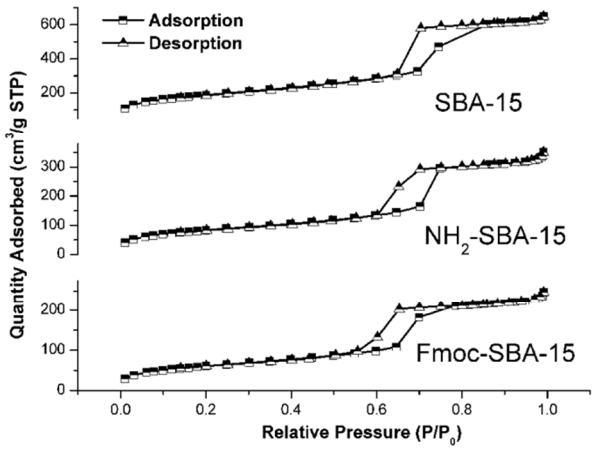

Fig. 3 N_2 adsorption-desorption isotherms of SBA-15, NH_2-SBA-15, and Fmoc-SBA-15.

FT-IR spectra

FT-IR spectroscopy was used to confirm the presence of APTES and lysine in the silicate framework. The FT-IR spectra for SBA-15, NH_2-SBA-15, and Fmoc-SBA-15 are shown in Fig. 4. The characteristic peaks around 1250–1000 and 3400 cm^{-1} are attributed to the Si-O-Si and -OH stretching vibrations, respectively. The stretching bands at 2870 and 2938 cm^{-1} are attributed to the asymmetric and symmetric C-H stretching in the aliphatic chains of both the aminopropyl groups in NH_2-SBA-15 and the lysine in Fmoc-SBA-15. The band at about 1560 cm^{-1} can probably be attributed to NH_2 bending, which was especially intense for NH_2-SBA-15 and Fmoc-SBA-15, indicating the presence of amino groups. The intense band at about 1679 cm^{-1} in the Fmoc-SBA-15 spectrum was attributed to the amide C=O group[40], which is important evidence for the presence of lysine. These results confirm that SBA-15 was successfully functionalized with APTES and lysine.

Table 1. Pore diameters (D_{BJH}), BET surface area (S_{BET}), and total pore volumes (V_{total}) for SBA-15, NH_2-SBA-15, and Fmoc-SBA-15 calculated from the N_2 adsorption–desorption isotherms.

Sample	S_{BET} (m^2 g)	D_{BJH} (Å)	V_{total} (cm^3 g)
SBA-15	675	65.5	0.96
NH_2-SBA-15	305	63.0	0.50
Fmoc-SBA-15	223	58.2	0.35

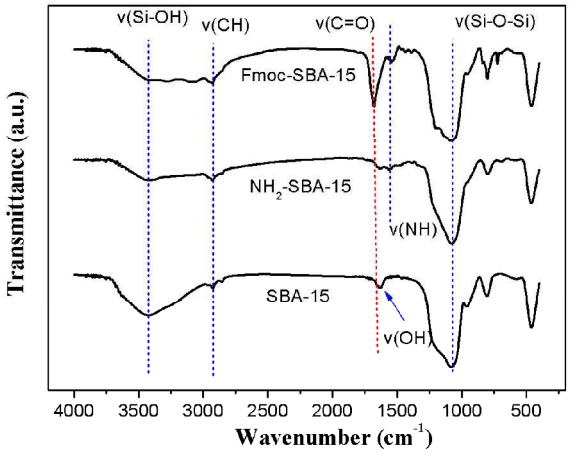

Fig. 4 FT-IR spectra of SBA-15, NH_2-SBA-15, and Fmoc-SBA-15.

Adsorption behaviour of REEs

Effect of solution pH and selective adsorption of Sc

In order to investigate the effect of the solution pH on the adsorption capacity of SBA-15, NH_2-SBA-15, and Fmoc-SBA-15, a set of adsorption experiments were performed using about 5 mg of adsorbent added into 20 mL of an aqueous solution containing 0.1 mg L^{-1} REE ions in the pH range of 1–7 with 1 h of stirring. The final pH values of the solution were measured after stirring and they were nearly the same as the initial pH values. For all three adsorbents (SBA-15, NH_2-SBA-15, and Fmoc-SBA-15) the metal uptake increased as the pH increased from 1 to 7. There was effectively no REE adsorption from solutions with low pH

(<5).

The highly concentrated hydrogen ions at low pH (<5) would directly compete with the REEs for active binding sites. Therefore, the higher REE adsorption rate for high-pH (7) solutions could be explained by the decrease in the competition between the protons (H^+) and the positively charged metal ions at the adsorbent surface sites[38].

Fig. 5 shows the selective adsorption of Sc on Fmoc-SBA-15. The REE adsorption rate was very low at pH 3 for all three adsorbents. However, only Fmoc-SBA-15 had high Sc adsorption rate (96%) and a low adsorption rate for the other REEs at pH 5. Therefore, at an appropriate pH, Fmoc-SBA-15 exhibited selective adsorption of Sc at a low concentration of REEs. This selective adsorption could be related to the strength of the interaction between the metal ions and the chemical groups (—NH_2 and C=O) in the adsorbent. Furthermore, the radius of the Sc ion is much lower than the radii of the other REE ions, leading to a greater polarization of the Sc ion. The strength of the interaction between the metal ions and the chemical groups in the adsorbent is probably proportional to the metal ion polarization, implying stronger bonding between the chemical groups and the Sc ions. Additionally, the number of sites occupied by H^+ on Fmoc-SBA-15 was higher than those for the other two adsorbents at pH 5 because there are more electron-attracting groups (—NH_2 and C=O) in the channel of Fmoc-SBA-15. Therefore, there were limited sites that could be occupied by other REEs on Fmoc-SBA-15.

Table 2 compares different Sc separation methods. The adsorption time of Fmoc-SBA-15 was much shorter for the method proposed here than for any other method, and distribution ratio was similar to those obtained for ion liquid extraction[20] and solvent extraction[42].

Table 2. Comparison of different Sc separation methods.

Method	Reagents	Time (min)	Distribution ratio D[a]	Ref.
Extraction chromatography	TRU Spec. resin/4 mol/L HCl	36	-	22
Ion chromatography	α-HIBA	120	-	21
Ion liquid extraction	[C8mim][PF6]/Cyanex 925	60	4.8	19
Ion liquid extraction	Cyanex925[A336][NO_3]/toluene	60	48	20
Extraction	Naphthenic acid diluted with isooctanol and sulphated kerosene	50	-	41
Solvent extraction	TVEX-DIOMP/ 4 mol/L HCl	1500	50	42
Adsorption	Fmoc-SBA-15	10	40	This work

[a] $D = \frac{[M]_t - [M]_a}{[M]_a}$, where $[M]_t$ and $[M]_a$ represent the initial and final concentrations of metal ions in the aqueous phase.

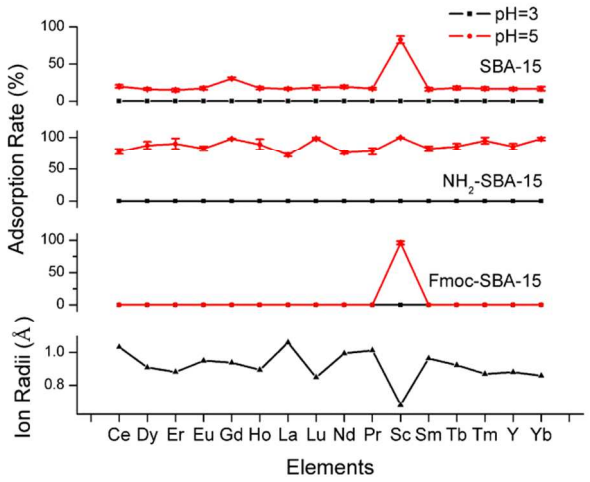

Fig. 5 Adsorption of REEs on SBA-15, NH_2-SBA-15, and Fmoc-SBA-15. Note the selective adsorption of Sc on Fmoc-SBA-15. Experimental conditions: adsorbent dose = 0.25 g L^{-1}, initial concentration of metal ion = 0.1 mg L^{-1}, and agitation time = 1 h.

Adsorption behaviour of Sc

Adsorption kinetics of Sc

The adsorption kinetics experiments were carried out for an initial Sc concentration of 20 mg L^{-1} and a pH of 5 for adsorption times between 2 min and 50 min with 5 mg Fmoc-SBA-15 adsorbent added into the 20 mL solution. Fig. 6 illustrates the kinetic process of Sc adsorption onto Fmoc-SBA-15. As shown, the adsorption capacity of Sc ions increased with time during the first 10 min until an equilibrium value was reached. The adsorption time of Fmoc-SBA-15 is shorter than those for other similar mesoporous materials reported in the literature[26,43-47]. During the initial 10 min, the Sc adsorption capacity of the Fmoc-SBA-15 increased, which clearly showed that the removal proceeded quickly. During the adsorption process, the C=O group was easily accessible and acted as an extremely effective adsorption site, because the uniform mesoporous channels of the SBA-15 most likely promoted the transportation of Sc ions.

Fig. 6 also shows the adsorption kinetics of Sc on the mesoporous Fmoc-SBA-15 adsorbent. We used the pseudo-first-order and pseudo-second-order models to fit the experimental adsorption kinetics data obtained from batch experiments in order to investigate the adsorption mechanisms. The fitting results for the different models are shown in Table 3. The value of q_e (20.39) calculated from the pseudo-second-order kinetic model agreed well with the experimental value (20.40). Moreover, the correlation coefficient value (0.9996) for the pseudo-second-order kinetic model was higher than that for pseudo-first-order kinetic model (0.8442), indicating that the pseudo-second-order model could perfectly express the adsorption kinetics of Sc on modified SBA-15 and the adsorption mechanism might be chemisorption.

Table 3. Comparison of pseudo-first-order and pseudo-second-order constants.

	Pseudo-first-order model			Pseudo-second-order model		
q_{eq} (exp) (mg·g^{-1})	k_1 (min^{-1})	q_{eq} (cal) (mg g^{-1})	R^2	k_2 (g (mg min)$^{-1}$)	q_{eq} (cal) (mg g^{-1})	R^2
20.40	0.0545	4.52	0.8442	0.0528	20.39	0.9996

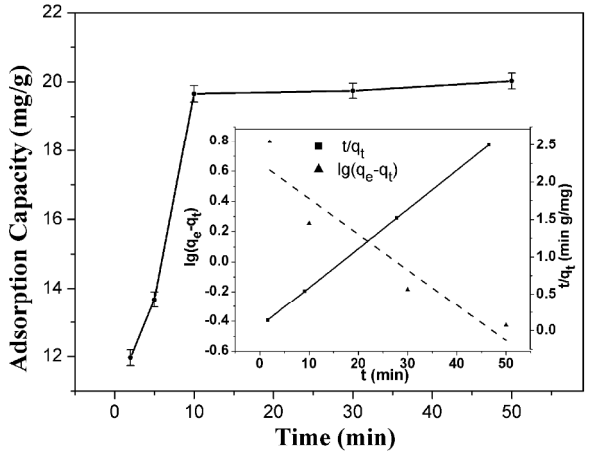

Fig. 6 Adsorption kinetics of Fmoc-SBA-15 in an aqueous solution of Sc. The inset shows the linear pseudo-first-order and pseudo-second-order kinetic plots. Conditions: adsorbent dose = 0.25 g L^{-1}, initial concentration of Sc ion = 20 mg L^{-1}, and pH = 5.

Adsorption isotherms of Sc

The Sc adsorption isotherms for Fmoc-SBA-15 are shown in Fig. 7. The initial concentrations of Sc ranged from 1 to 60 mg L^{-1}. To each solution, 5 mg of adsorbent was added, and the solution was intensively mixed at room temperature. The solutions were adjusted so that the pH was 5. In the low-concentration region, the Sc adsorption capacities were proportional to their initial concentrations. At higher concentrations, the increase in the adsorption capacities was retarded, and the maximum Sc adsorption capacity of Fmoc-SBA-15 of 35.29 mg g^{-1} was reached, which is higher than the values obtained from acetylacetone-modified silica gel[15] and benzamide-modified silica gel[16].

In order to describe the Sc adsorption behaviour on Fmoc-SAB-15, two classical adsorption models, namely, the Langmuir and Freundlich models, were applied to the measured data. The Langmuir model describes monolayer adsorption on a homogeneous, flat adsorbent surface, and the Freundlich model describes the adsorption on a heterogeneous surface.

The linearized Langmuir and Freundlich plots are given in Fig. 7, and the adsorption constants are summarized in Table 4. As shown in Table 4, the Langmuir model fits the adsorption data better than the Freundlich model, which is evident from the higher correlation coefficient (R^2 = 0.9921). These results demonstrate the homogeneous nature of the Sc binding on Fmoc-SBA-15.

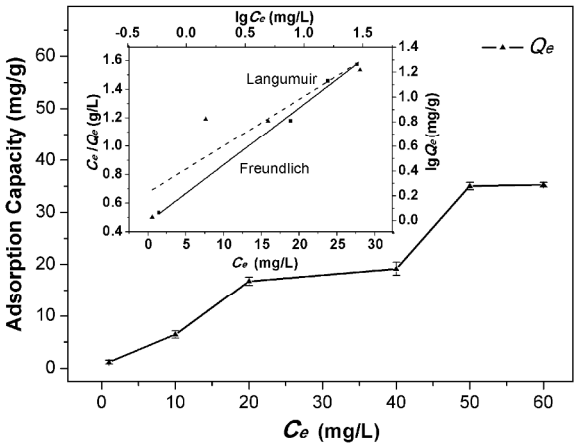

Fig. 7 Adsorption isotherms for Sc on Fmoc-SBA-15. The inset shows the linear Langmuir and Freundlich plots. Experimental conditions: adsorbent dose = 0.25 g L^{-1}, solution volume = 20 mL, initial concentration of Sc ions = 1–60 mg L^{-1}, and pH = 5. *Ce* (mg L^{-1}) is the concentration of the solute.

Table 4. Langmuir and Freundlich isotherm constants.

Langmuir adsorption isotherm	Freundlich adsorption isotherm
q_{max} = 30.5064	K_F =1.6704
b =0.0487	n = 1.3893
R^2 = 0.7026	R^2 =0.9921

CONCLUSIONS

For the first time, we have synthesized a novel organic–inorganic mesoporous composite with a well-ordered mesoporous structure combining NH_2-SBA-15 and lysine. Because it had a high selectivity toward Sc, our composite material could be a suitable adsorbent for separating Sc from REEs. Under the optimum experimental conditions, Sc adsorption by Fmoc-SBA-15 follows pseudo-second-order reaction kinetics and the Freundlich adsorption isotherm. In addition, the maximum Sc adsorption capacity of Fmoc-SBA-15 was 35.29 mg g^{-1}. Therefore, Fmoc-SBA-15 could be a promising adsorbent for the preconcentration of Sc and in the separation of Sc.

ACKNOWLEDGEMENTS

The financial support of the National Natural Science Foundation of China (No. 21175145) and the Shanghai Committee of Science and Technology (No. 13142201200) is gratefully acknowledged.

Notes and references

[a]*School of Material Science and Engineering, Shanghai University, Shanghai 200444, China.*

[b]*Shanghai Institute of Ceramics, Chinese Academy of Sciences, Shanghai 200050, China.*

**Corresponding author: Tel: 86-21-52413503; Fax: (+86)21-52413016; E-mail: wangzheng@mail.sic.ac.cn; Address: 1295 Dingxi Road Shanghai, 200050 P. R. China.*

REFERENCES

1. S.Y. Liu, Rare Metals and Cemented Carbides, 1995, 2, 57-61.
2. G.Y. Guo, Y.L. Chen, Y. Li, JOM, 1988, 40, 28-31.
3. W.W. Wang, Y. Pranolo, C.Y. Cheng, Hydrometallurgy, 2011, 108, 100-108.
4. L.K. Gao, Y. Chen, Journal of Rare Earths, 2010, 28, 622-626.
5. L.D. Aquino, M. Morgana, M.A. Carboni, M. Staiano, M.V. Antisari, M. Re, M. Lorito, F. Vinale, K.M. Abadi, S.L. Woo, Soil Biol. Biochem, 2009, 41, 2406-2413.
6. N.R. Šmuc, T. Dolenec, T. Serafimovski, M. Dolenec, P. Vrhovnik, Geoderma, 2012, 183-184, 1-11.
7. L. Miao, Y.L. Ma, R.S. Xu, W. Yan, Environ. Earth Sci., 2011, 63, 501-511.
8. X.F. Li, Z.B. Chen, Z.Q. Chen, Y. Zhang, Chemosphere, 2013, 93, 1240-1246.
9. A.A. Shaltout, M.I. Khoder, A.A. El-Abssawy, S.K. Hassan, D.L.G. Borges, Environ. Pollut., 2013, 178, 197-201.
10. J. Feng, H. Zhang, W.F. Zhu, C.Q. Liu, S.Q. Xu, D.S. Wu, Journal of Rare Earths, 2000, 18, 356-359.
11. Z.Y. Chen, J. Ecol. Rural Environ., 2005, 21, 72-73.
12. Z.Y. Chen, X.D. Zhu, J. Ecol. Rural Environ. 2008, 24, 88-91.
13. W.F. Zhu, S.Q. Xu, P.P. Shao, H. Zhang, D.S. Wu, W.J. Yang, J. Feng, L. Feng, Biol. Trace Elem. Res., 2005, 104, 1-7.
14. P. Arvela, B.V. Lehmann, O. Grajewski, E. Oberdisse, Experientia, 1980, 36, 860-861.
15. N. Zhang, C.Z. Huang, B. Hu, Anal. Sci., 2007, 23, 997-1002.
16. L.J. Zhang, X.J. Chang, Y.H. Zhai, Q. He, X.P. Huang, Z. Hu, N. Jiang, Anal. Chim. Acta, 2008, 629, 84–91.
17. J. Jerez, A. C. Isaguirre, C. Bazán, L. D. Martinez, S. Cerutti, Talanta, 2014, 124, 89-94.
18. A. A. Levinson, Introduction to Exploration Geochemistry, Applied Publishing Ltd, Wilmette, Illinois, USA, 1980.
19. X.Q. Sun, D.B. Wu, J. Chen, D.Q. Li, J. Chem. Technol. Biotechnol., 2007, 82,267-272.
20. X.Q. Sun, Y. Ji, L. Guo, J. Chen, D.Q. Li, Sep. Purif. Technol., 2011, 81, 25-30.
21. R. Dybczyń ski, K. Kulisa, Chromatographia, 2005, 61,573-580.
22. H. Minowa, M. Ebihara, Anal. Chim. Acta, 2003, 498, 25-37.
23. K.J. Eisentraut, D.J. Griest, R.E. Sievers, Anal. Chem., 1971, 43, 2003-2006.
24. Y. Sohrin, S. Urushihara, S. Nakatsuka, T. Kono, E. Higo, T. Minami, K. Norisuye, S. Umetani, Anal. Chem., 2008, 80, 6267-6273.
25. Y.B. Zhu, T. Umemura, H. Haraguchi, K. Inagaki, K. Chiba, Talanta, 2009, 78, 891-895.
26. W.L. Guo, R. Chen, Y. Liu, M.J. Meng, X.G. Meng, Z.Y. Hu, Z.L. Song, Colloids Surf., A., 2013, 436, 693-703.
27. Y. Liu, Z.C. Liu, J. Gao, J.D. Dai, J. Han, Y. Wan, J.M. Xie, Y.S. Yan, J. Hazard. Mater., 2011, 186, 197-205.
28. E. Da'na, A. Sayari, Desalination, 2012, 285, 62-67.
29. C. McManamon, A.M. Burke, J.D. Holmes, M.A. Morris, J. Colloid Interface Sci., 2012, 369, 330-337.
30. J. Huang, M. Ye, Y.Q. Qu, L.F. Chu, R. Chen, Q.Z. He, D.F. Xu, J. Colloid Interface Sci., 2012, 385, 137-146.
31. A.M. Liu, K. Hidajat, S. Kawi, D.Y. Zhao, Chem. Commun., 2000, 13, 1145-1146.
32. M. Mureseanu, A. Reiss, I. Stefanescu, E. David, V. Parvulescu, G. Renard, V. Hulea, Chemosphere, 2008, 73, 1499-1504.
33. X.G. Wang, K.S.K. Lin, J.C.C. Chan, S. Cheng, J. Phys. Chem. B, 2005, 109, 1763-1769.
34. Z.F. Gao, L.N. Wang, T. Qi, J.L. Chu, Y. Zhang, Colloids Surf., A, 2007, 304, 77-81.
35. L.X. Zhang, C.C. Yu, W.R. Zhao, Z.L. Hua, H.G. Chen, L. Li, J.L. Shi, J. Non-Cryst. Solids, 2007, 353, 4055-4061.
36. Z. Wang, D.M. Fang, Q. Li, L.X. Zhang, R. Qian, Y. Zhu, H.Y. Qu, Y.P. Du, Anal. Chim. Acta, 2012, 725, 81-86.
37. Q. Li, Z. Wang, D.M. Fang, H.Y. Qu, Y. Zhu, H.J. Zou, Y.R. Chen, Y.P. Du, H.L. Hu, New J. Chem., 2014, 38, 248-254.
38. A. Shahbazi, H. Younesi, A. Badiei, Chem. Eng. J., 2011, 68, 505-518.
39. Z.J. Liang, B. Fadhel, C.J. Schneider, A.L. Chaffee, Microporous Mesoporous Mater., 2008, 111, 536-543.
40. D. Haldar, Tetrahedron, 2008, 64, 186 -190.
41. C.S. Liao, J.T. Jia, Y. Zhang, G. Xu, C.H. Yan, B.G. Li, G.X. Xu, J. Alloys Compd., 2001, 323–324, 833–837.
42. V. Korovin, Y. Shestak, Hydrometallurgy, 2009, 95, 346–349.
43. J.S. Li, X.Y. Miao, Y.X. Hao, J.Y. Zhao, X.Y. Sun, L.J. Wang, J. Colloid Interface Sci., 2008, 318, 309–314.
44. F.Q. An, B.J. Gao, X. Dai, M. Wang, X.H. Wang, J. Hazard. Mater., 2011, 192, 956–962.
45. M. Mureseanu, N. Cioatera, I. Trandafir, I. Georgescu, F. Fajula, A. Galarneau, Microporous Mesoporous Mater., 2011, 146, 141–150.
46. S. Asuha, X.G. Zhou, S. Zhao, J. Hazard. Mater., 2010, 181, 204–210.
47. Y.J. Jiang, Q.M. Gao, H.G. Yu, Y.R. Chen, F. Deng, Microporous Mesoporous Mater., 2007, 103, 316–324.

Graphical Abstract

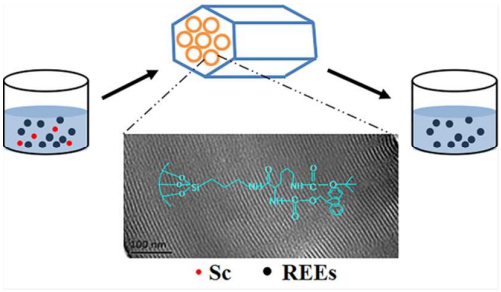

A novel lysine-functionalized mesoporous material was synthesized using a facile two-step post-grafting method, selectively adsorbing scandium from aqueous solution.